PREDICTION OF THE CREEP BEHAVIOUR OF A 21CR-11NI-0.17N STEEL BASED ON CONSTANT STRESS CREEP TESTS

E. Gariboldi*, J. Schwertel†, H. Stamm†

A series of creep tests at 973 K under constant stress condition were carried out to characterise the high temperature behaviour of 21Cr-11Ni-0.17N austenitic stainless steel. In addition, constant load and a variable stress creep test were performed. Microstructural observations on crept specimens showed the presence of intergranular and surface cracks. Constant stress creep curves were used to determine the material parameters of a viscoplastic constitutive model based on a backstress and continuum damage approach. The predictive capabilities were checked by its application to load controlled creep tests and a test with variable stresses. The description of constant stress or constant load creep conditions is fairly good. The model satisfactorily describes also sudden load changes.

INTRODUCTION

Creep tests are usually performed under constant load conditions. The strain rate increase of the tertiary creep stage consists of a part due to the reduction of the cross section, leading to an increase of the true stress, and a part due to microstructural damage effects. These effects like intergranular cracking, cavities etc. increase the effective stress to which the specimen is exposed. To extract properly the damage effects, constant stress creep tests have to be performed. This holds especially for materials experiencing large deformations.

A series of constant stress creep tests was performed using a high-temperature austenitic stainless steel. The resulting creep curves were modelled by a viscoplastic constitutive model including a damage variable. The predictive capabilities of the model were tested by a comparison with constant load and variable stress tests.

EXPERIMENTAL PROCEDURE AND RESULTS

Material. Avesta 253MA, a high-temperature stainless steel corresponding to the ASTM S30815 grade, was investigated. The chemical composition is given in Table 1. The steel was hot rolled to bars with a diameter of 20 mm, annealed at

* Dipartimento di Meccanica, Politecnico di Milano,
† Joint Research Centre - Institute for Advanced Materials - Ispra

1070 °C, water cooled and descaled. The alloy microstructure was found to be austenitic with a mean grain size of 60 μm.

TABLE 1: Chemical composition of the steel (wt. %).

C	Si	Mn	Cr	Ni	Mo	P	S	N	Ce	Fe
0.09	1.7	0.6	20.80	10.90	0.18	0.022	0.0008	0.16	0.03	bal.

Creep tests. A series of ten uniaxial tests were carried out. The experiments were performed on a servo-mechanical electronic creep machine MAYES TC30E. Cylindrical specimens with a diameter of 8 mm and a gauge length of 50 mm were used. Six constant stress (A-F) and three constant load (G-I) experiments together with a test under variable stress levels (J, see also Fig. 4) were performed. The experiments were carried out in air at 973 K under initial stresses ranging from 114 to 200 MPa. The corresponding times to rupture ranged from 45 to over 1000 h. Some tests were interrupted during the secondary or tertiary creep stage. The experimental conditions and the main results are summarised in Table 2.

TABLE 2: Experimental data from the creep tests. I indicates the interruption of the test, R the final rupture; σ and F stress and load control respectively, σ_0 the initial stress, $\dot{\varepsilon}_{min}$ and $\dot{\varepsilon}_{min\,m}$ the measured and predicted minimum true strain rate, t_f and t_{fm} the real and predicted time to rupture, t_i the interruption time, ε_{cf} the final creep strain, *RA* the area reduction for the broken specimens.

#	*mode*	σ_0	R/I	$\dot{\varepsilon}_{min}$ [s^{-1}]	$\dot{\varepsilon}_{min\,m}$ [s^{-1}]	ε_{cf}	t_i, t_f [h]	t_{fm} [h]	*RA* [%]
A	σ	114	I	$1.11 \cdot 10^{-8}$	$2.30 \cdot 10^{-8}$	0.002	33	-	-
B	σ	120	I	$2.00 \cdot 10^{-8}$	$2.97 \cdot 10^{-8}$	0.003	36	-	-
C	σ	120	R	$1.53 \cdot 10^{-8}$	$2.97 \cdot 10^{-8}$	0.148	1032	1090	20.05
D	σ	150	R	$1.25 \cdot 10^{-7}$	$1.38 \cdot 10^{-7}$	0.173	250	250	22.81
E	σ	170	R	$3.53 \cdot 10^{-7}$	$3.29 \cdot 10^{-7}$	0.168	98	112	23.05
F	σ	198	R	$7.83 \cdot 10^{-7}$	$9.46 \cdot 10^{-7}$	0.168	45	42	23.17
G	F	120	I	$3.89 \cdot 10^{-8}$	$3.16 \cdot 10^{-8}$	0.045	232	-	-
H	F	120	R	$4.53 \cdot 10^{-8}$	$3.16 \cdot 10^{-8}$	0.182	416	703	26.72
I	F	170	R	$3.40 \cdot 10^{-7}$	$3.84 \cdot 10^{-7}$	0.207	84	69	24,40
J	stress change		I	$1.62 \cdot 10^{-7}$	$1.38 \cdot 10^{-7}$	0.109	169	-	-

Results of creep tests. The measured creep curves (Figure 1) showed short primary and secondary creep stages. Tertiary creep strain started early during the tests and gradually increased up to the final rupture. The broken specimens did not show necking or marked strain localisation (see the *RA* values in Table 2).

Microstructural observations. Microstructural and fractographic analyses have been carried out on the fracture surfaces and on a longitudinal section of each specimen. All broken specimens showed an intergranular fracture mode. Intergranular microcracks were also found along the whole gauge length on the

specimen surface. This type of surface damage was also observed when the creep tests were interrupted during the tertiary creep range (G and J). Metallographic examinations of the sections (see Figure 2) showed microcracks consisting of one or more cracked grain boundary facets with a tendency to coalesce to longer cracks in the vicinity of the rupture surface.

MODELLING OF THE CREEP CURVES

Model. The following viscoplastic constitutive model has been applied for the description of the creep curves:

$$\dot{\varepsilon} = A[\sigma/(1-D)-\alpha]^n \,\mathrm{sign}[\sigma/(1-D)-\alpha] \tag{1}$$

$$\dot{\alpha} = h|\alpha|^{-\beta}\dot{\varepsilon} - R|\alpha|^{n-\beta}\,\mathrm{sign}(\alpha) \tag{2}$$

$$\dot{D} = C\sigma^{\nu}/(1-D)^{\mu} \tag{3}$$

In these equations $\dot{\varepsilon}$ symbolises the inelastic strain rate, α the internal stress (kinematic hardening variable, backstress) which has been introduced to model the primary creep stage, and D a damage variable. A,n,h,R,β,ν,μ and C are material parameters which must be determined from the experimental data.

This model is similar to the viscoplastic model of Robinson [1] and has been combined with a damage model of the Kachanov type [2]. The evolution law (2) consists of a dynamic hardening and a time-dependent recovery term which reduces hardening. For D=0 (undamaged state) α increases with time and reaches a saturation value $\alpha_s=(h/R\cdot\varepsilon_{min})^{1/n}$. This implies that $\dot{\varepsilon}$ decreases until the constant value $\dot{\varepsilon}_{min}$ is reached. The growth of D increases the effective stress $\sigma/(1\text{-}D)$ and therefore $\dot{\varepsilon}$. In the case of σ=const., i.e., when a stress-controlled creep test is performed, eq. (3) can be solved explicitly resulting in

$$D = 1-[1-t/t_f]^{1/(1+\mu)} \quad \text{with} \quad t_f = [C\sigma^{\nu}(1+\mu)]^{-1}. \tag{4}$$

For $D\rightarrow 1$ $\dot{\varepsilon}$ becomes infinite and fracture takes place at the rupture time t_f.

Determination of the material parameters. The constant stress creep experiments were used for the parameter evaluation. A numerical minimisation procedure, described in [3], was applied which minimises the weighted sum of the squares of the difference between measured and calculated inelastic strains. Due to the nonlinearity of the equations, a two-step minimisation procedure had to be applied. Firstly, only data before the tertiary regime were fitted assuming D=0. The values for the parameters A,n,h,R and β resulted from this first fit. In a second step the complete curves, including the tertiary part (D>0), were considered to determine the parameters C, μ and ν. Table 3 contains the results of the minimisation procedure.

TABLE 3: Material parameters for Avesta 253MA at 973°C

A [$h^{-1}MPa^{-n}$]	n	h[$MPa^{\beta+1}$]	R [$h^{-1}MPa^{\beta-n+1}$]	β	C [$MPa^{-\nu}s^{-1}$]	ν	μ	E [MPa]
$1.06\cdot10^{-15}$	6.77	$2.71\cdot10^{12}$	$4.94\cdot10^{-5}$	4.42	$1.10\cdot10^{-18}$	6.37	49.5	129600

DISCUSSION AND CONCLUSIONS

Figure 3 shows the failure times t_f vs. σ_0 for both stress and load controlled tests. The values for the constant stress tests are very well fitted by the straight line. This line follows from equations (1)-(3) and does not exactly coincide with the linear regression line for the constant stress test data. Values for the load-controlled tests are below those of the stress-controlled ones due to the increase of the true stress.

A comparison between experimental and theoretical creep curves is performed in Figure 1, where the fitted constant stress curves are drawn together with the predicted constant load curves. The agreement between theory and measurement is very good if the usual experimental scattering is taken into consideration. The curvature of the creep curves cannot be fitted for all stresses in the same quality. In particular large scattering is observed for the two 120 MPa tests. The large failure time of the stress-controlled test G could be explained by the occurrence of intra- and intergranular precipitates observed in samples aged at 700 °C for up to 1000 hours. As previously reported by Sandström and Maode [4,5] for creep tests performed at 750 °C, the presence of such secondary phases could reduce the creep ductility of the steel in long term creep tests.

Figure 4 compares measured and predicted results of the test with stress changes (test J). For an easier comparison the experimental and predicted strains were both shifted to zero at t=63 h. It can be observed that the model predicts the overall material behaviour quite well even for this particular load history. During the first stress reduction period starting at t=66 h a distinct increase of the strain can be seen whereas for the third reduction at t=75 h a contraction of the specimen despite a tensile stress takes place. In this latter case σ is smaller than α and therefore the strain rate is negative. Both effects are underestimated by the model. Additionally, after each new increase of the stress, the model predicts a primary creep behaviour in contrast to the experiment. All these discrepancies are due to an underestimation of the recovery rate of the backstress, i.e., in the case of stress reduction the effective stress σ-α is initially too small whereas it becomes too large after stress increases. However, it must be emphasized that the model is capable to reproduce the observed phenomena after load changes and gives a very good prediction of the strain changes.

In summary, the model allows a fairly good description of the material behaviour with respect to the description of the primary and secondary creep ranges and the prediction of the rupture times. Further investigations will be carried out to improve the modelling for the damage-induced tertiary creep. Particularly, non-destructive ultrasonic velocity measurements and quantitative metallography methods will be applied to assess the local damage state of each specimen [6].

REFERENCES

[1] D.N. Robinson, P.A. Bartolotta, NASA-CR 174836, 1985.

[2] L.M. Kachanov, Izv.Akad.Nauk.S.S.R., Otd. Tekh. Nauk., Vol. 8, 1958, pp. 26-31.

[3] J. Schwertel, VDI Fortschritt-Berichte, Reihe 5, Nr.306, 1993.

[4] R. Sandström, Y. Maode, Proc. Creep and Fracture of Engineering Materials and Structures, 1987, pp. 427-439.

[5] Y. Maode , R. Sandström, Avesta Corrosion Management, 1 (1989)

[6] H. Stamm, P. Hähner, J. Schwertel, Proc. Int. Conf. on Computational Engineering Science, July 30-August 3, 1995, Hawaii, Springer, Berlin, pp. 1330-1335

ACKNOWLEDGEMENT

The authors thank Mr G. Ferrari from Avesta Sheffield for granting the examined material.

FIGURES

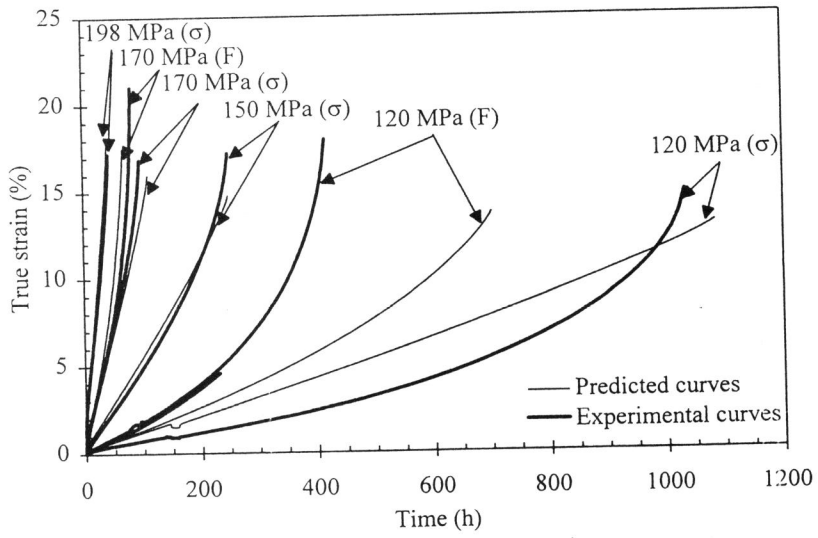

Figure 1. Comparison between measured and predicted creep curves. The strains are the true ones. (σ) and (F) signify stress and load controlling.

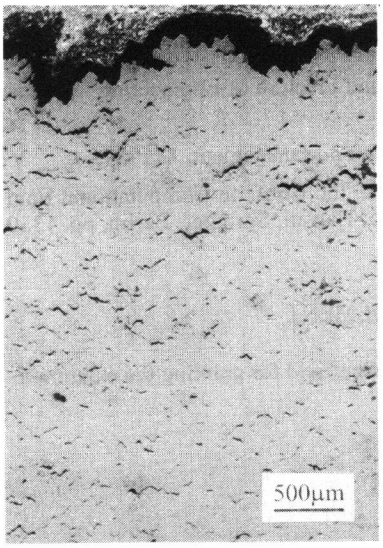

Figure 2. Microstructural features near the rupture zone (test C, σ vertical).

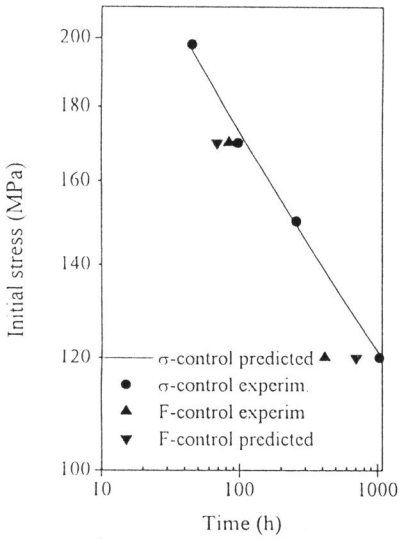

Figure 3. Measured and predicted rupture times.

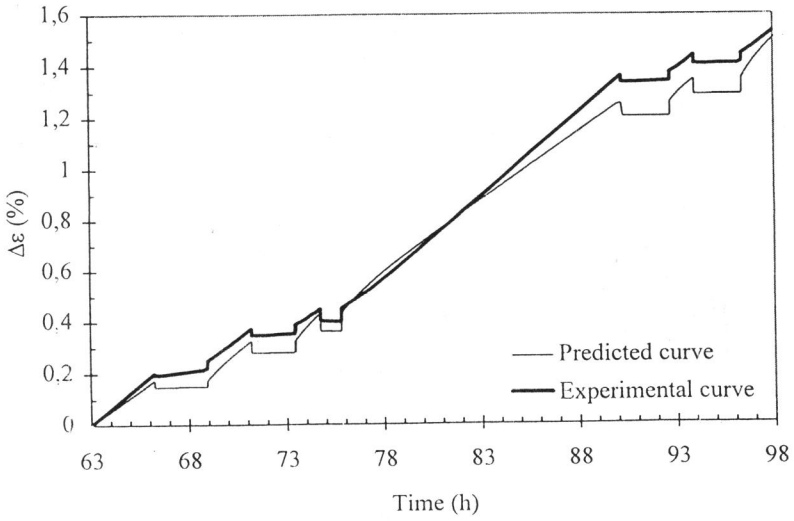

Figure 4. Experimental and predicted behaviour for test J.